Glacial ocean overturning intensified by tidal mixing in a global circulation model

Glacial ocean overturning intensified by tidal mixing in a global circulation model

A. Schmittner[1], J. A. M. Green[2], and S.-B. Wilmes[2]

[1]College of Earth, Ocean, and Atmospheric Sciences, Oregon State University, Corvallis, Oregon, USA, [2]School of Ocean Sciences, Bangor University, Menai Bridge, UK

Abstract Due to lower sea levels during the Last Glacial Maximum (LGM), tidal energy dissipation was shifted from the shallow margins into the deep ocean. Here using a high-resolution tide model, we estimate that global energy fluxes below 200 m depth were almost quadrupled during the LGM. Applying the energy fluxes to a consistent tidal mixing parameterization of a global climate model results in a large intensification of mixing. Global mean vertical diffusivity increases by more than a factor of 3, and consequently, the simulated meridional overturning circulation accelerates by ~21–46%. In the model, these effects are at least as important as those from changes in surface boundary conditions. Our findings contrast with the prevailing view that the abyssal LGM circulation was more sluggish. We conclude that changes in tidal mixing are an important mechanism that may have strongly increased the glacial deep ocean circulation and should no longer be neglected in paleoclimate simulations.

1. Introduction

During the Last Glacial Maximum (LGM) (23,000–19,000 years before present), Earth's climate was colder [*Annan and Hargreaves*, 2013], ice sheets covered North America and northern Europe, and sea level was about 130 m lower than it is today [*Clark et al.*, 2009]. The LGM is one of the best studied time periods in Earth's history. Still, its ocean's meridional overturning circulation (MOC), although important for global heat, carbon, nutrient, and other fluxes, remains a topic of contention [*Lynch-Stieglitz et al.*, 2007]. The prevailing view of the recent literature is one of a sluggish abyssal circulation that is less ventilated and has accumulated more respired carbon [e.g., *DeVries and Primeau*, 2010; *Sigman et al.*, 2010; *Skinner et al.*, 2010]. Climate model simulations, such as those from the Paleoclimate Modeling Intercomparison Project, typically consider various changes in boundary conditions, but they do not account for differences in ocean mixing, despite its importance for the MOC [*Bryan*, 1987], and they produce conflicting results [*Green et al.*, 2009; *Otto-Bliesner et al.*, 2007]. A recent climate modeling study, assuming reduced deep ocean mixing during the LGM, concludes to have identified unambiguously the mechanism for observed large millennial time scale climate variability (Dansaard-Oeschger oscillations) [*Peltier and Vettoretti*, 2014]. Here we suggest that vertical mixing during the LGM was enhanced, and not reduced, thus questioning the conclusions of this study as well as the prevailing idea of a sluggish abyssal circulation during the LGM [*DeVries and Primeau*, 2010; *Sigman et al.*, 2010; *Skinner et al.*, 2010].

Mass fluxes across density layers in the upwelling part of the global MOC require an energy source to overcome gravity. In the contemporary, ocean tides are important [*Huang*, 1999; *Munk and Wunsch*, 1998], providing 3.5 TW (1 TW = 10^{12} W) globally, but most of this energy is lost to bottom friction on the shallow continental shelves (~0–200 m depth) with minor impacts on the MOC, which is controlled by mixing in the thermocline (~200–1000 m) and deep ocean (below 1 km). Only about 1–1.5 TW of tidal energy is dissipated below about 200 to 500 m depths [*Egbert and Ray*, 2000; *Schmittner and Egbert*, 2014], almost entirely through tidal flow over rough topography, which generates internal waves, the breaking of which leads to turbulence and mixing [*Jayne and St. Laurent*, 2001; *Ledwell et al.*, 2000; *St. Laurent et al.*, 2002]. During the LGM, much of the shallow tidal energy sink was removed because continental shelves were exposed due to the sea level drop. This must have generated larger tides and more dissipation in the deep ocean, which has triggered speculations that the LGM MOC must have been stronger than today [*Green et al.*, 2009; *Wunsch*, 2003].

Tide model simulations confirm larger LGM tides and suggest that energy dissipation of the major M_2 tide was globally about 50% larger during the LGM and tripled in the deep ocean [*Egbert et al.*, 2004; *Green*, 2010;
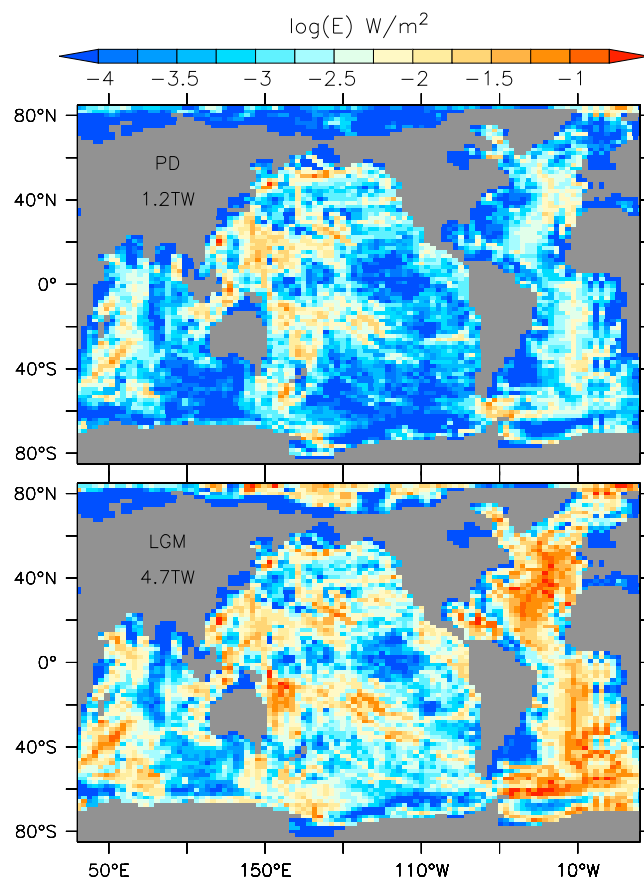
Figure 1. Maps of tidal energy dissipation due to internal wave drag E_w as a function of longitude (horizontal axis) and latitude (vertical axis). The sum of the dissipations of the four major tidal constituents (M_2, S_2, K_1, and O_1) calculated by the tide model for the (top) present day and the (bottom) LGM mapped onto the climate model grid is shown. The numbers over Asia denote the global integrals.

Wilmes and Green, 2014]. This implies much more vigorous deep ocean mixing and a stronger MOC. However, *Montenegro et al.* [2007] (M07), using a relatively coarse (0.5°) horizontal resolution tide model and the University of Victoria (UVic) climate model, report small changes in mixing and no consistent effects on the Atlantic MOC transport (M07 did not present other MOC aspects). Here we use a higher resolution tide model and an improved tidal mixing parameterization in a global climate-ocean circulation model to reassess this issue. We also consider additional MOC aspects not reported in M07.

2. Models and Experiments

A quasi-global tide model [*Wilmes and Green*, 2014] at 0.125° resolution (see Methods section for details) estimates energy fluxes $E_{TC} = E_{b,TC} + E_{w,TC}$ due to bottom drag E_b (important in the shallow ocean) and internal wave drag E_w (dominating at depths) from four major tidal constituents $TC \in (M_2, S_2, K_1,$ and $O_1)$. Together they account for more than 94% of today's dissipation [*Egbert and Ray*, 2003]. Various parameterizations for E_w have been proposed; see *Green and Nycander* [2013] for a recent review and comparison. Here we use a modified

version of *Zaron and Egbert*'s [2006] scheme. For our first simulations, we applied a statistical fit to global present-day observations to obtain a globally averaged vertical stratification (described in terms of the buoyancy frequency $N = \sqrt{-g/\rho \partial \rho/\partial z}$, where g is the gravitational acceleration, ρ is the potential density, and z is the depth). In the second iteration runs presented in the supporting information, the parameterization was modified to use a spatially varying N computed from the climate model output. The main results from our study are likely insensitive to the specific internal wave drag parameterization used, because the spatial distributions of E_w are all similar for the different parameterizations [*Green and Nycander*, 2013]. The resulting horizontal distributions of E_w (Figure 1) are used as input to a tidal mixing parameterization in the global climate model [*Schmittner and Egbert*, 2014]. The UVic model (see Methods section for details) uses a three-dimensional ocean circulation model coupled to a simple one-layer energy-moisture balance model of the atmosphere. This setup allows multiple, 4500 yearlong sensitivity experiments, but it excludes wind or cloud interactions, that is, wind stress in the momentum forcing of the surface ocean and sea ice, advection velocities used in the horizontal transport of humidity, wind speed used in the air-sea gas and heat exchange, and atmospheric albedo are prescribed according to a mean annual cycle from reanalysis data.

Results from the last 500 years from three climate model experiments are presented: one present-day (preindustrial) control simulation (PD) and two LGM simulations. Both LGM runs use the same basic boundary conditions: prescribed ice sheets [*Peltier*, 2004], orbital parameters (which impact the seasonal and latitudinal distributions of solar irradiance), and atmospheric carbon dioxide concentrations (185 ppm, in
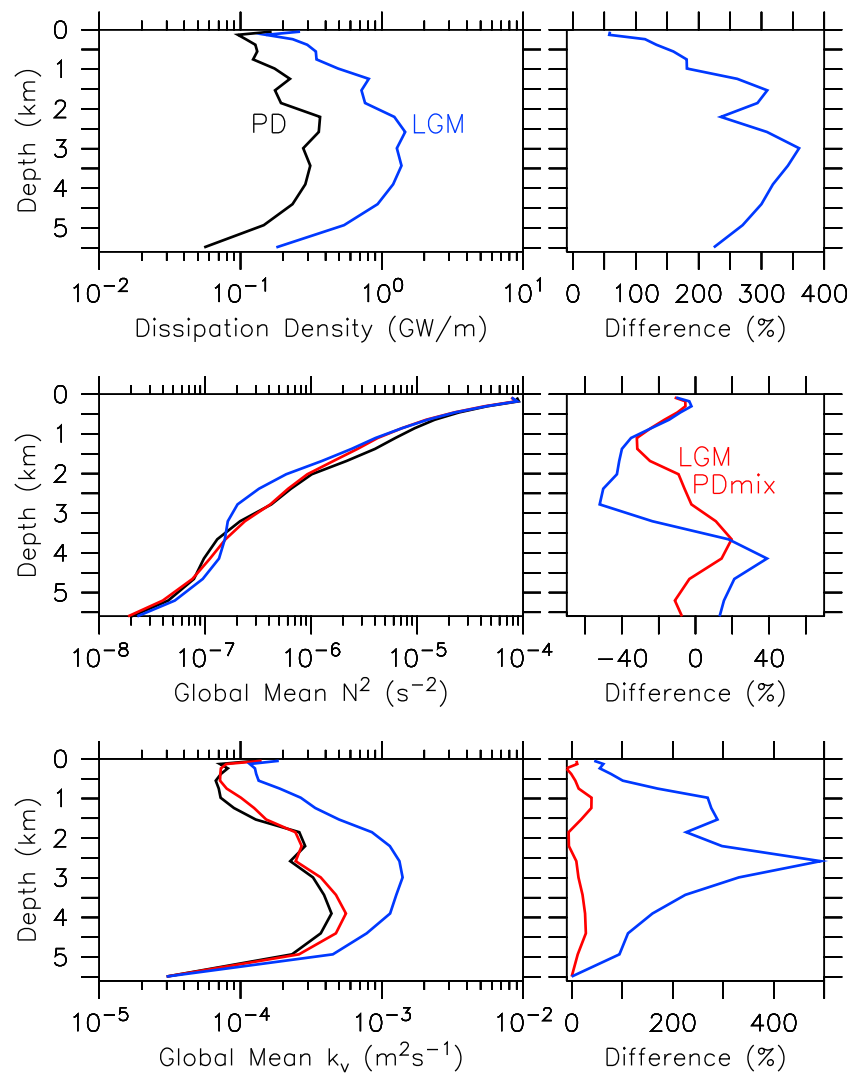
Figure 2. Vertical distributions of globally horizontally integrated (top) tidal energy dissipation density $E_w/\Delta z$ (per model layer thickness Δz) mapped on the climate model grid, (middle) averaged squared buoyancy frequency, and (bottom) averaged diapycnal diffusivity for the present day (black), LGM with PD mixing (red), and LGM (blue) experiments. (left) Absolute values and (right) percent differences with respect to PD (e.g., (LGM − PD)/PD × 100). N^2 was calculated using density referenced to 1 km depth (σ_1).

contrast to the 280 ppm concentrations of the PD; changes in minor greenhouse gases are neglected here). PD bathymetry is used in all climate model runs. The only difference between them is the tidal energy input E_w. Experiment "LGM PDmix" uses the present-day flux (Figure 1, top), whereas "LGM" (Figure 1, bottom) uses the flux from the tide model LGM simulation with lowered sea level but present-day stratification.

3. Results

The LGM tide model simulates a large intensification in tidal energy fluxes, with global total dissipation rates surging from 3.7 TW to 5.8 TW, consistent with previous studies [*Egbert et al.*, 2004; *Wilmes and Green*, 2014], whereas E_w almost quadruples from 1.3 TW to 4.7 TW (Table S1 in the supporting information and Figure 1). This implies that dissipation due to bottom drag decreased from 2.4 TW at PD to only 1.1 TW at the LGM, consistent with the reduced area covered by shallow oceans. Virtually all of the E_w enhancement occurs in the lower thermocline and deep ocean (below 200 m). Increases are particularly pronounced in the North Atlantic due to resonance effects [*Egbert et al.*, 2004; *Green*, 2010] (Figure 1).
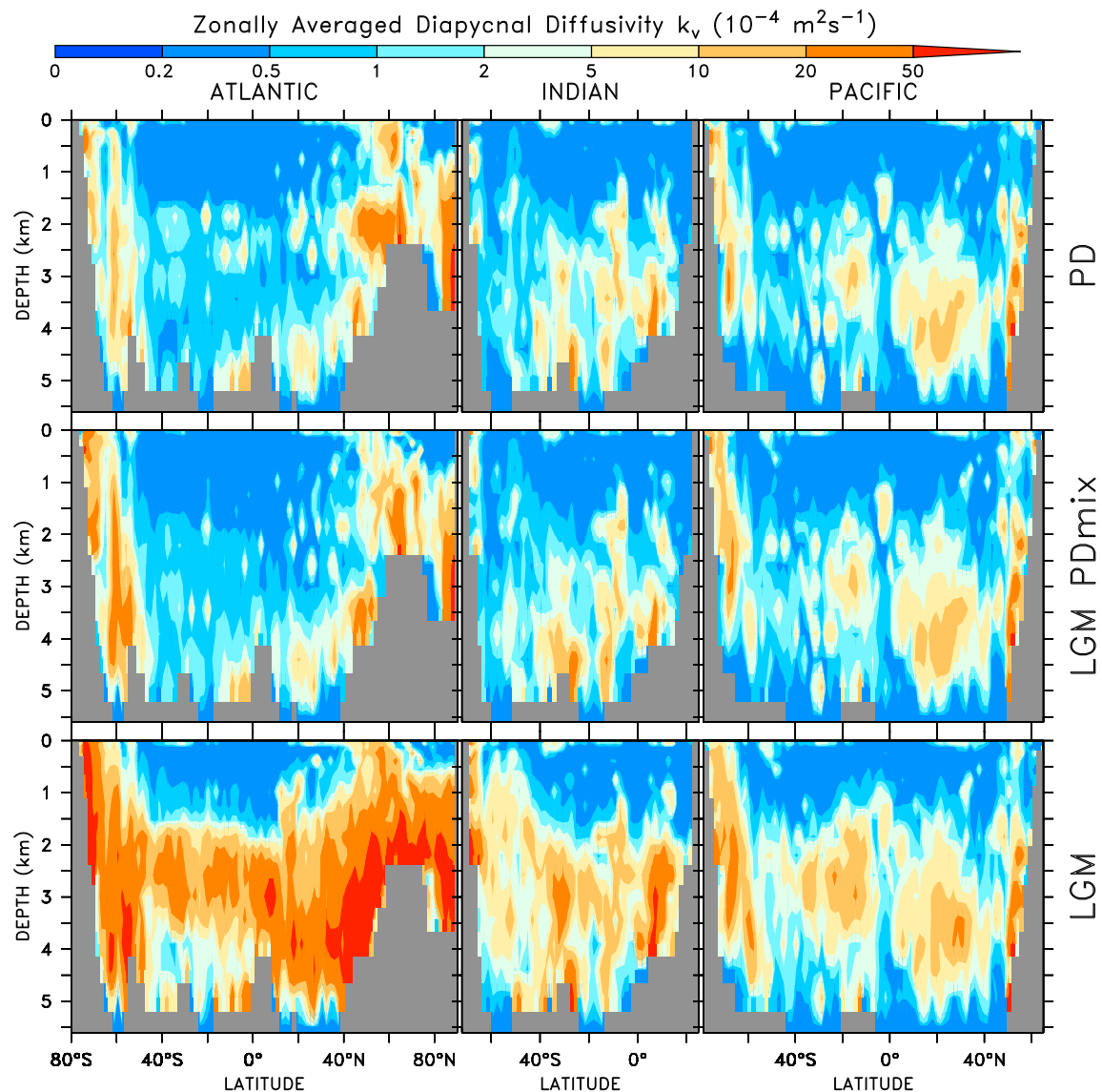
Figure 3. Zonally averaged diffusivities in the (left) Atlantic, (middle) Indian, and (right) Pacific at equilibrium in experiments (top) PD, (middle) LGM PDmix, and (bottom) LGM.

Horizontally integrated dissipation density increases at all depths but more so in the deep ocean than at the surface (Figure 2). At middepth, it is about 4 times larger in the LGM case compared with PD. Changes in stratification (N^2) are much smaller than those in dissipation. N^2 decreases slightly in both LGM simulations in the lower thermocline and middepths due to changes in surface boundary conditions. Increased mixing in the LGM simulation with respect to the LGM PDmix case causes a cooling of the upper ~2 km and a warming at depth (not shown), at least partially due to a deepening and increased flux of North Atlantic Deep Water (NADW), which decreases stratification between 2 and 3 km and increases it below 3.5 km.

Horizontally averaged diffusivities k_v increase substantially at all depths if LGM dissipation is used, whereas changes are much smaller for PD dissipation (Figure 2, bottom). Global mean k_v values are 2.1, 2.4, and 7.3 (all in $10^{-4}\,m^2\,s^{-1}$) for PD, LGM PDmix, and LGM, respectively. This indicates that changes in stratification have a much smaller impact on diffusivities than changes in dissipation. This conclusion is also supported by additional experiments exploring feedback between stratification, dissipation, and circulation (supporting information). The most dramatic increases in mixing occur in the Atlantic (by ~650% on average), whereas in the Indian (~320%) and Pacific (~190%), they are slightly more modest (Figure 3).
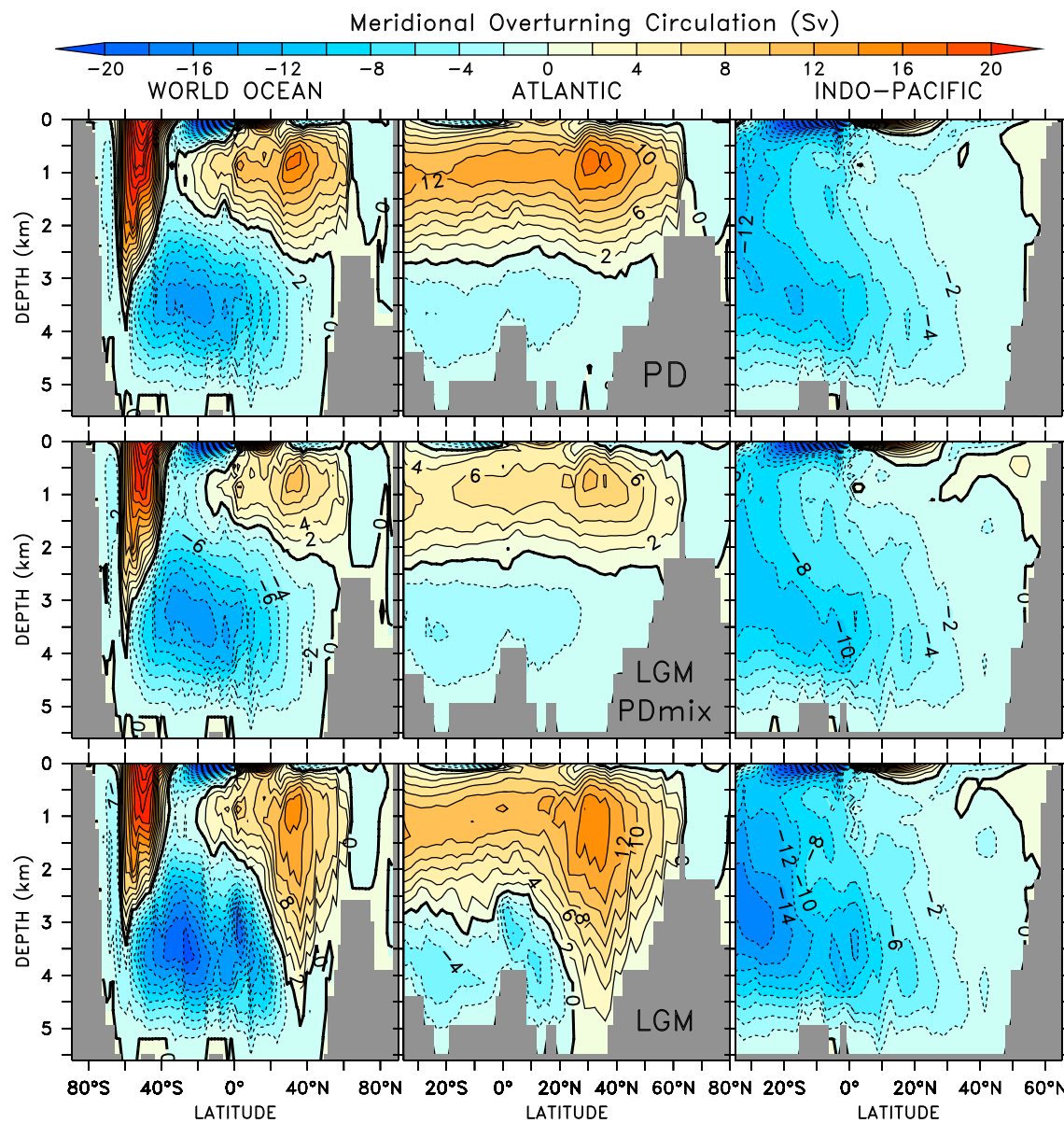
Figure 4. Meridional overturning circulation stream function of the (left) world ocean, (middle) Atlantic, and (right) Indian and Pacific in experiments (top) PD, (middle) LGM PDmix, and (bottom) LGM.

Changes in buoyancy forcing alone (LGM PDmix) lead to a large decrease (by 41–49%) of the middepth Atlantic MOC (AMOC) cell in our model (Figure 4 and Table S2 in the supporting information), consistent with previous results [*Weaver et al.*, 2001]. Circumpolar Deep Water (CPDW) inflow from the Southern Ocean into the Indian Ocean also decreases in LGM PDmix (by 30%), whereas the deep cells associated with Antarctic Bottom Water (AABW) flow into the Atlantic (0%) and CPDW flow into the Pacific (+6%) do not change much.

Including tidal mixing in the LGM simulations (experiment LGM versus LGM PDmix) leads to a large intensification of the MOC in the climate model. In the North and South Atlantic, the middepth overturning cell associated with NADW increases by 36% and 46%, respectively, almost entirely compensating for the decreases due to buoyancy forcing. (The reported percentage changes are with respect to the stronger MOC state in order to be comparable to the values reported for the buoyancy forcing; see also Table S2's caption in the supporting information.) AABW in the Atlantic accelerates by

21%, and CPDW fluxes into the Indian Ocean and Pacific increase by 32% and 24%, respectively. Thus, while for the AMOC, mixing effects are similar (albeit of opposite sign and slightly smaller) compared to buoyancy effects, for AABW and Pacific bottom water flow, mixing effects are much larger than buoyancy effects.

4. Discussion

The lower resolution tide model without Antarctic ice shelves and with a different internal wave drag parameterization used by M07 shows much smaller changes in dissipation (their Figure 1) than those simulated by our model (Figure S1 in the supporting information), particularly in the Atlantic. Changes there are likely sensitive to the resolved bathymetry owing to resonance effects [*Egbert et al.*, 2004]. We infer that M07's small change in global E_w is the main reason for the differences with our results even though we cannot exclude other reasons. The results may also be sensitive to the choice of the internal wave drag parameterization. Differences in the k_v parameterization used in the climate model could also play a role. Quantification of these possibilities will be an important task for future research.

In their two simulations of glacial climate, *Peltier and Vettoretti* [2014] used values of k_v *smaller than or similar to* those used for their modern simulations: one globally constant value of $0.17 \times 10^{-4} \, \text{m}^2 \, \text{s}^{-1}$ and one fixed vertical profile varying from $0.17 \times 10^{-4} \, \text{m}^2 \, \text{s}^{-1}$ at the surface to $1 \times 10^{-4} \, \text{m}^2 \, \text{s}^{-1}$ below ~1 km depth. These values are much smaller than the averaged values suggested by our LGM simulation (10^{-4}–$10^{-3} \, \text{m}^2 \, \text{s}^{-1}$; Figure 2), and they are inconsistent with our results of *increased* LGM diffusivities compared to modern.

The parameterization of tidal mixing used here assumes that only a small constant fraction (1/3) of the energy dissipated into the internal wavefield contributes to local mixing. The remainder (2/3) propagates away and dissipates elsewhere, which is reflected in the constant background diffusivity $k_{bg} = 0.3 \times 10^{-4} \, \text{m}^2 \, \text{s}^{-1}$. Given the large increase in tidal energy dissipation during the LGM, it is reasonable to assume that the energy dissipation in regions far from the internal wave generation sites would also increase. However, this was not considered in our simulations in which the background diffusivity was fixed. Thus, our estimate of changed tidal energy dissipation on k_v and the LGM MOC is conservative.

5. Conclusions

We conclude that large increases in tidal energy dissipation in the deep ocean during the LGM may have intensified the MOC's middepth and bottom flows. In our climate model, tidal mixing effects are more important than those from surface buoyancy fluxes, particularly for bottom flows. The effect of tidal mixing on the AMOC in our model (~+40%) is larger than the combined effects of bouyancy and momentum fluxes as simulated by most comprehensive models (~−20 to +40%) [*Otto-Bliesner et al.*, 2007]. Assuming that reconstructions of a weakened LGM AMOC are true, one can infer that the combined effects of other forcings would need to lead to a weakening of the AMOC. Our simulated LGM circulation including LGM mixing is not realistic because it shows deeper NADW, whereas tracer distributions such as carbon isotopes indicate similar or shallower NADW flow [*Gebbie*, 2014]. This mismatch suggests that other forcings, and/or model responses to the forcings, are not correct and/or that transient effects played a role [*Green et al.*, 2009; *Zhang et al.*, 2013]. Closure of the Bering Strait due to sea level drop leads to less freshwater transport from the Pacific into the Arctic/Atlantic and hence a strengthening of the LGM AMOC [*Hu et al.*, 2010]. In our model, this effect is not included because the Bering Strait is closed in both PD and LGM simulations. This raises the question which process(es) could counter the effects of enhanced mixing and the closed Bering Strait to produce the weaker and shallower AMOC implied by the reconstructions. Answering this question and reconciling paleoobservations with models will require more work.

Our model does not reproduce the high abyssal salinities inferred from South Atlantic sediments [*Adkins et al.*, 2002], which may imply stronger stratification. The effects of realistic LGM stratification deserve careful assessment in future work, but here we note that effects on mixing and the MOC are not straightforward due to opposing effects of N on dissipation (equation (M2)) and k_v (equation (M5)). However, while our experiments show only small effects of changes in stratification (LGM PDmix versus PD; see also Table S3 and Figure S3 in the supporting information), the effects may be larger for more realistic LGM stratification.

Our findings are in contrast to the prevailing view that the abyssal circulation was more sluggish during the LGM [*DeVries and Primeau*, 2010; *Sigman et al.*, 2010; *Skinner et al.*, 2010], and they question far-reaching conclusions from a study in which LGM mixing was reduced [*Peltier and Vettoretti*, 2014].

6. Materials and Methods

We use tidal energy dissipation maps calculated from a tide model as input to a parameterization of tidal mixing used in the climate model.

6.1. Tide Model Description

The tidal simulations are based on those in *Wilmes and Green* [2014]—a further development of the model used by *Egbert et al.* [2004]. The model, OTIS, solves the linearized shallow water equations on a $0.125° \times 0.125°$ horizontal grid with an open boundary at 89°N. In the current simulations, data from TPXO7.2 are used to provide boundary conditions in the PD simulations, whereas the LGM simulations used a vertical wall at the northern boundary to eliminate uncertainties with the boundary forcing. The effects of this should be minimal as any modification of the conditions here will only have marginal effects on the large-scale tidal dynamics [*Wilmes and Green*, 2014]. The only other forcing is the astronomic tide-generating force. Momentum is dissipated through two processes: first, a quadratic (in velocity) bed friction term

$$\mathbf{F}_b = C_d \mathbf{U}|\mathbf{u}|/H, \tag{M1}$$

in which $C_d = 3 \times 10^{-3}$ is a drag coefficient, H is the depth of the seafloor, $\mathbf{U} = \mathbf{u}H$ is the tidal transport vector, and $\mathbf{u}$ is the total tidal velocity from all constituents under consideration, and second, a linear transfer of energy to internal waves. The latter is based on the scheme given by *Zaron and Egbert* [2006] but with an allowance of a spatially varying stratification field $N(x,y,z)$ which comes from the climate model simulations:

$$\mathbf{F}_w = C|\nabla H|^2 \frac{N_H \overline{N}}{8\pi^2 \omega} \mathbf{U}, \tag{M2}$$

where $C = 2$ is a scaling factor, N_b is the buoyancy frequency at the bed, N is the depth-averaged buoyancy frequency, and ω is the tidal frequency. The corresponding energy dissipation for bottom drag is

$$E_b = \rho_0 C_d |\mathbf{u}|\mathbf{u}^2 \tag{M3}$$

and that for internal wave drag

$$E_w = \rho_0 C|\nabla H|^2 \frac{N_b \overline{N}}{8\pi^2 \omega} H\mathbf{u}^2. \tag{M4}$$

Dissipation was computed by using modeled tidal velocity amplitudes in the respective parameterization, and the resulting (high-resolution) fields were averaged over 28×14 grid points before being adjusted to the UVic grid using linear interpolation.

6.2. Climate Model Description

The University of Victoria Earth System Climate Model [*Weaver et al.*, 2001] is used in version 2.9 [*Eby et al.*, 2009]. It consists of a coarse resolution ($1.8 \times 3.6°$, 19 vertical layers) ocean general circulation model coupled to a one-layer atmospheric energy-moisture balance model and a dynamic thermodynamic sea ice model, both at the same horizontal resolution. The model is forced with seasonally varying solar irradiance at the top-of-the-atmosphere, cloud albedo, wind stress, and moisture advection velocities. This seasonal forcing does not change between different years. We use the tidal mixing parameterization developed by *Jayne and St. Laurent* [2001], *Simmons et al.* [2004], and *St. Laurent et al.* [2002] as improved by *Schmittner and Egbert* [2014], which includes the effect of subgrid-scale bathymetry on the depth of energy input and distinguishes between diurnal and semidiurnal tides. Briefly, the diapycnal diffusivity is

$$k_v = k_{bg} + \frac{\Gamma \varepsilon}{N^2}, \tag{M5}$$

where $k_{bg} = 0.3 \times 10^{-4}\,\mathrm{m^2\,s^{-1}}$ is the background diffusivitiy accounting for the effects of remotely dissipated tidal energy and other mixing processes, N is the buoyancy frequency, and $\Gamma = 0.2$ is the mixing efficiency. The energy dissipation rate is

$$\varepsilon = \frac{1}{\rho} \sum_{z'>z}^{H} \sum_{\mathrm{TC}} q_{\mathrm{TC}} E_{w,\mathrm{TC}}(x, y, z') F(z, z'), \tag{M6}$$

where $E_{w,\mathrm{TC}}(x,y,z')$ is the energy flux from the barotropic tide into the internal wavefield calculated from the tide model and mapped onto a climate model grid considering subgrid-scale bathymetry at high horizontal resolution (which introduced the z' dependence); F is the vertical decay function, which uses an e-folding depth of 500 m above the seafloor H; and

$$q_{\mathrm{TC}} = \begin{cases} 1, & \text{for } |y| > y_{c,\mathrm{TC}} \\ 0.33, & \text{else} \end{cases} \tag{M7}$$

is the local dissipation efficiency, which depends on the critical latitude y_c, which is 30° for diurnal tides (K_1 and O_1) and 70° for semidiurnal tides (M_2 and S_2).

References

Adkins, J. F., K. McIntyre, and D. P. Schrag (2002), The salinity, temperature, and delta O-18 of the glacial deep ocean, *Science*, *298*(5599), 1769–1773.

Annan, J. D., and J. C. Hargreaves (2013), A new global reconstruction of temperature changes at the Last Glacial Maximum, *Clim. Past*, *9*(1), 367–376.

Bryan, F. (1987), Parameter sensitivity of primitive equation ocean general circulation models, *J. Phys. Oceanogr.*, *17*(7), 970–985.

Clark, P. U., A. S. Dyke, J. D. Shakun, A. E. Carlson, J. Clark, B. Wohlfarth, J. X. Mitrovica, S. W. Hostetler, and A. M. McCabe (2009), The Last Glacial Maximum, *Science*, *325*(5941), 710–714.

DeVries, T., and F. Primeau (2010), An improved method for estimating water-mass ventilation age from radiocarbon data, *Earth Planet. Sci. Lett.*, *295*(3–4), 367–378.

Eby, M., K. Zickfeld, A. Montenegro, D. Archer, K. J. Meissner, and A. J. Weaver (2009), Lifetime of anthropogenic climate change: Millennial time scales of potential CO_2 and surface temperature perturbations, *J. Clim.*, *22*(10), 2501–2511.

Egbert, G. D., and R. D. Ray (2000), Significant dissipation of tidal energy in the deep ocean inferred from satellite altimeter data, *Nature*, *405*(6788), 775–778.

Egbert, G. D., and R. D. Ray (2003), Semi-diurnal and diurnal tidal dissipation from TOPEX/Poseidon altimetry, *Geophys. Res. Lett.*, *30*(17), 1907, doi:10.1029/2003GL017676.

Egbert, G. D., R. D. Ray, and B. G. Bills (2004), Numerical modeling of the global semidiurnal tide in the present day and in the Last Glacial Maximum, *J. Geophys. Res.*, *109*, C03003, doi:10.1029/2003JC001973.

Gebbie, G. (2014), How much did Glacial North Atlantic Water shoal?, *Paleoceanography*, *29*, 190–209, doi:10.1002/2013PA002557.

Green, J. A. M. (2010), Ocean tides and resonance, *Ocean Dyn.*, *60*(5), 1243–1253.

Green, J. A. M., and J. Nycander (2013), A comparison of tidal conversion parameterizations for tidal models, *J. Phys. Oceanogr.*, *43*(1), 104–119.

Green, J. A. M., C. L. Green, G. R. Bigg, T. P. Rippeth, J. D. Scourse, and K. Uehara (2009), Tidal mixing and the meridional overturning circulation from the Last Glacial Maximum, *Geophys. Res. Lett.*, *36*, L15603, doi:10.1029/2009GL039309.

Hu, A., G. A. Meehl, B. L. Otto-Bliesner, C. Waelbroeck, W. Han, M.-F. Loutre, K. Lambeck, J. X. Mitrovica, and N. Rosenbloom (2010), Influence of Bering Strait flow and North Atlantic circulation on glacial sea-level changes, *Nat. Geosci.*, *3*(2), 118–121.

Huang, R. X. (1999), Mixing and energetics of the oceanic thermohaline circulation, *J. Phys. Oceanogr.*, *29*(4), 727–746.

Jayne, S. R., and L. C. St. Laurent (2001), Parameterizing tidal dissipation over rough topography, *Geophys. Res. Lett.*, *28*(5), 811–814, doi:10.1029/2000GL012044.

Ledwell, J. R., E. T. Montgomery, K. L. Polzin, L. C. St. Laurent, R. W. Schmitt, and J. M. Toole (2000), Evidence for enhanced mixing over rough topography in the abyssal ocean, *Nature*, *403*(6766), 179–182.

Lynch-Stieglitz, J., et al. (2007), Atlantic meridional overturning circulation during the Last Glacial Maximum, *Science*, *316*(5821), 66–69.

Montenegro, A., M. Eby, A. J. Weaver, and S. R. Jayne (2007), Response of a climate model to tidal mixing parameterization under present day and Last Glacial Maximum conditions, *Ocean Model.*, *19*(3–4), 125–137.

Munk, W., and C. Wunsch (1998), Abyssal recipes II: Energetics of tidal and wind mixing, *Deep Sea Res., Part I*, *45*(12), 1977–2010.

Otto-Bliesner, B. L., C. D. Hewitt, T. M. Marchitto, E. Brady, A. Abe-Ouchi, M. Crucifix, S. Murakami, and S. L. Weber (2007), Last Glacial Maximum ocean thermohaline circulation: PMIP2 model intercomparisons and data constraints, *Geophys. Res. Lett.*, *34*, L12706, doi:10.1029/2007GL029475.

Peltier, W. R. (2004), Global glacial isostasy and the surface of the ice-age Earth: The ICE-5G (VM2) model and GRACE, *Annu. Rev. Planet. Sci.*, *32*, 111–149.

Peltier, W. R., and G. Vettoretti (2014), Dansgaard-Oeschger oscillations predicted in a comprehensive model of glacial climate: A "kicked" salt oscillator in the Atlantic, *Geophys. Res. Lett.*, *41*, 7306–7313, doi:10.1002/2014GL061413.

Schmittner, A., and G. D. Egbert (2014), An improved parameterization of tidal mixing for ocean models, *Geosci. Model Dev.*, *7*(1), 211–224.

Sigman, D. M., M. P. Hain, and G. H. Haug (2010), The polar ocean and glacial cycles in atmospheric CO(2) concentration, *Nature*, *466*(7302), 47–55.

Simmons, H. L., S. R. Jayne, L. C. St. Laurent, and A. J. Weaver (2004), Tidally driven mixing in a numerical model of the ocean general circulation, *Ocean Model.*, *6*(3–4), 245–263.

Skinner, L. C., S. Fallon, C. Waelbroeck, E. Michel, and S. Barker (2010), Ventilation of the deep Southern Ocean and deglacial CO_2 rise, *Science*, *328*(5982), 1147–1151.

St. Laurent, L. C., H. L. Simmons, and S. R. Jayne (2002), Estimating tidally driven mixing in the deep ocean, *Geophys. Res. Lett.*, *29*(23), doi:10.1029/2002GL015633.

Weaver, A. J., et al. (2001), The UVic Earth System Climate Model: Model description, climatology, and applications to past, present and future climates, *Atmos. Ocean*, *39*(4), 361–428.

Wilmes, S.-B., and J. A. M. Green (2014), The evolution of tides and tidally driven mixing over 21,000 years, *J. Geophys. Res. Oceans*, *119*, 4083–4100, doi:10.1002/2013JC009605.

Wunsch, C. (2003), Determining paleoceanographic circulations, with emphasis on the Last Glacial Maximum, *Quat. Sci. Rev.*, *22*(2–4), 371–385.

Zaron, E. D., and G. D. Egbert (2006), Estimating open-ocean barotropic tidal dissipation: The Hawaiian Ridge, *J. Phys. Oceanogr.*, *36*(6), 1019–1035.

Zhang, X., G. Lohmann, G. Knorr, and X. Xu (2013), Different ocean states and transient characteristics in Last Glacial Maximum simulations and implications for deglaciation, *Clim. Past*, *9*(5), 2319–2333.